

# DATA-DRIVEN PROCESS ANALYSIS FOR IRON FOUNDRIES WITH AUTOMATIC SAND MOLDING PROCESS

**Chinnadit Baitiang** 

Technical University of Munich, Garching, Germany  
TUM School of Engineering and Design, Department of Mechanical Engineering, Chair of Metal Forming and Casting,  
Munich, Germany  
RWP GmbH, Bundesstraße 77, 52159 Roetgen, Germany

**Konrad Weiß**

RWP GmbH, Bundesstraße 77, 52159 Roetgen, Germany

**Mathias Krüger**

Ortrander Eisenhütte GmbH, Königsbrücker Straße 10-12, 01990 Ortrand, Germany

**Wolfram Volk and Philipp Lechner**

Technical University of Munich, Garching, Germany  
TUM School of Engineering and Design, Department of Mechanical Engineering, Chair of Metal Forming and Casting,  
Munich, Germany

Copyright © 2023 The Author(s)  
<https://doi.org/10.1007/s40962-023-01080-z>

## Abstract

*This paper proposes a methodological framework to develop a data-driven process control using pure industrial production data from a cast iron foundry, despite the limitation of complete casting traceability. The aim is to help sand foundries to produce good castings. A reference foundry, which produces mainly automotive and oven parts with automatic sand molding and pouring machines, was selected. Past data, where only good castings were produced, were extracted from the database to determine parameter control limits (upper and lower control limits) with the aid of statistical approach. To identify critical process parameters associated with casting defects, process data from the zero and high scrap production batches were systematically compared. This method clearly identified unstable parameters without exact synchronization*

*between inline and part quality data. Molding sand moisture, temperature and compactability, liquidus temperature of the melt, phosphorus content, carbon equivalent and pouring temperature were found to be the critical parameters to be stabilized. Finally, a regression model for predicting and controlling of molding sand moisture and liquidus temperature of the melt was created. The determined boundaries and the models were helpful for the foundry in assisting ongoing production control and correction of process inputs to achieve target casting quality.*

**Keywords:** cast iron, sand casting, casting defects, process data, regression analysis, process control

## Introduction

In recent years, several foundries have been running their production process with modern machinery together with

inline sensors, enabling continuous process monitoring and control. Consequently, a decent amount of casting process data has been generated and collected by foundries, especially those with automatic molding and pouring processes. The aim has always been to gain useful information out of these data to improve existing process control and to avoid casting defects. Despite the available data, many sand

foundries are still faced with high rate of defective parts and are looking for a robust solution from the data.

In the past, several approaches for analyzing the reason of casting defects were introduced such as cause–effect diagrams and statistical approaches.<sup>1,2</sup> In addition, many works presented the use of machine learning methods, e.g. artificial neural network, to find the cause and predict the occurrence of casting defects.<sup>3,4</sup> In general, machine learning approaches require large amount of process data, while some foundries try to reduce measurement costs, resulting in insufficient data. In addition, to develop a robust process control in industrial practice, not only the causal parameters should be identified but also what in the process should be adjusted and by how much. In other words, some target functions for these parameters and an appropriate operating range should be determined. The problem is that most of these data-based approaches require a proper experimental setup for accurate links between inline data and quality data of the outgoing castings, which is not currently the case for most sand foundries. There have been several published works and commercial tools, proposing casting traceability solution for foundries. Vedel-Smith et al. introduced a direct part marking during the molding process using reconfigurable pin-type tooling integrated into the pattern-plate.<sup>5</sup> Similarly, DISA TAG (Trace and Guidance), a pattern-integrated automatic marking system with rotating dials, was introduced by Norican Group.<sup>6</sup> In addition, SinterCast introduced SinterCast Cast Tracker which uses labeling of cores, combined with RFID tag of each flask to provide complete part traceability.<sup>7</sup> However, due to cost reasons, not all sand foundries are convinced to invest further in implementing a fully traceable process. In our view, there should be an optional solution for these foundries to make use of their collected data. The authors, therefore, propose a new methodology to identify critical process parameters and develop a robust process control for sand foundries that have been collecting process data but without full traceability.

## Materials and Methods

In this work, a large set of green sand casting production data collected during the years 2018–2021 was provided by Ortrander Eisenhütte GmbH, one of the most modern sand foundries for machine-molded iron castings in Europe. The foundry produces various cast iron products (part weight of up to 35 kg) such as automotive and stove parts with an annual production capacity of around 23,000 tons. The cast materials are gray cast iron (GJL), vermicular cast iron (GJV) and nodular cast iron (GJS). The annual rejection rate was 5–7%. The typical casting defects found were gas bubbles, sand inclusions, porosities, cold run and broken molds. The inline process data (molding, melting and pouring parameters) were recorded with the date and time

of measurement and the name of the corresponding cast product. The date of pouring (but not the time of pouring) are annotated on each casting. The number of defective parts per day for each cast product was documented with information on the defect group. Similar to most sand foundries, all these collected data do not allow an exact link between a specific piece of part and its inline data. For instance, it is not possible to point out the actual value of molding sand properties, chemical composition or pouring temperature of a found defective part. With these conditions, it is not feasible either to obtain quantifiable correlations in the data or to model the process directly with statistics or machine learning approaches, and this is where our approach aims to assist. Before going through our method, the authors first introduce the casting process and the parameters that the foundry collects.

## Description of Casting Process and Collected Data

The foundry produces cast products using the green sand casting process with automatic vertical molding and pouring lines. The production process starts with the preparation of molding sand and molten iron. The molding sand is prepared by two sand mixers, each of which supplies approximately 4 tons of molding sand to all three molding machines every 2 minutes via a conveyor, as shown in Figure 1. The main compositions of molding sand mixture are silica sand, bentonite, water and sea coal. The molten iron is prepared with four induction melting furnaces, each with a capacity of 6 tons, treated with magnesium if required and then transported by forklift to feed the three induction-heated pouring furnaces. In the molding machines, the prepared molding sand is blown into a vertical molding chamber and pressed through two patterns to form a piece of mold with two different side shapes. The finished mold is then pushed out of the chamber. This process step is repeated with a cycle time of 15–20 seconds (depending on the weight and the number of castings in the mold), forming a continuous chain of frameless molds that are transported on a conveyor to the pouring furnace. The molds are then filled with molten iron from the pouring furnace and moved further along the conveyor at the same speed as the molding process. From this stage, solidification and cooling of the castings take place. At the end of molding line, the castings are separated from the sand molds on the shakeout conveyor (shakeout process) and cleaned with shot blast machines. The used sand from the shakeout process is transported to a sand recycling plant for reuse in the future production with recycling rate of 99%. Finally, the quality of each outgoing cast part is proved by means of visual inspection, and the number of defective parts is documented. Every half an hour, a piece of the cast part is randomly taken for mechanical property testing.

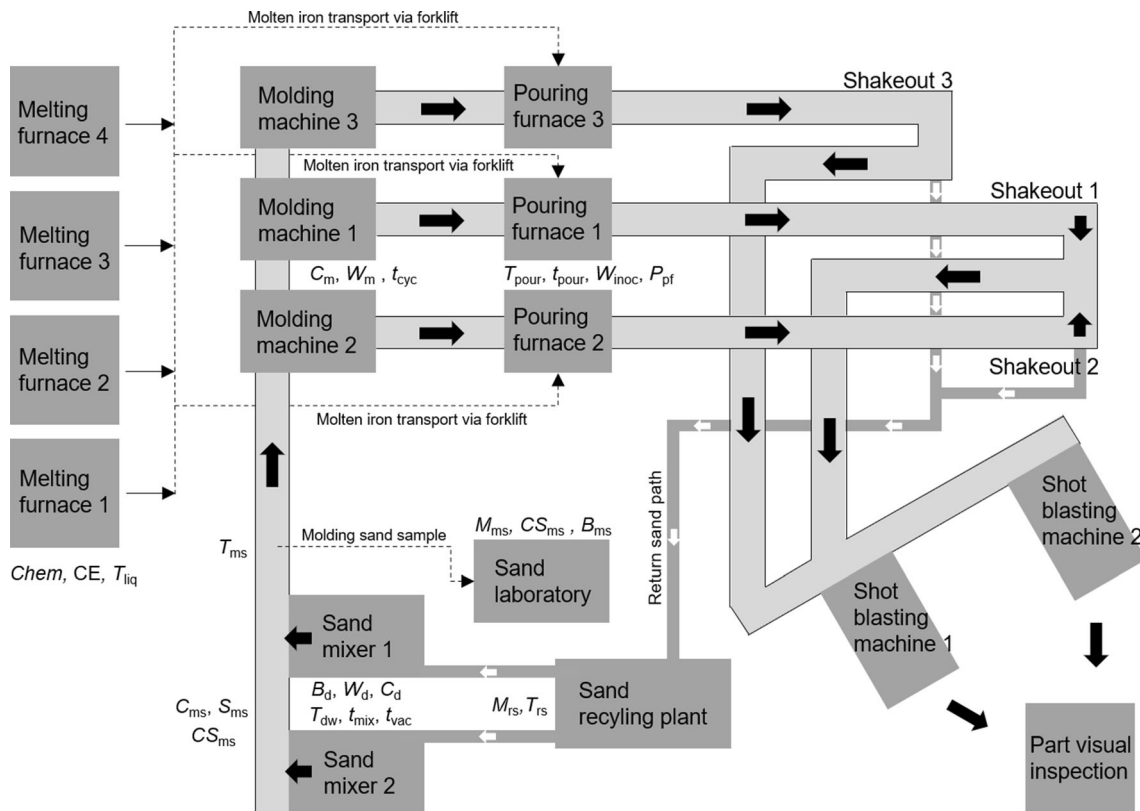


**Figure 1. Layout of green sand casting process with three automatic molding lines.**

For process control purpose, continuous measurement of the process parameters listed in Table 1 is carried out by various sensors, machines and measuring devices. Several molding sand parameters are measured inline by the sand mixers, molding sand testers, molding machines and offline by sand laboratory equipment. The chemical composition and other properties of the melt are inspected by spectrometer and thermal analysis (TA). All these data are stored in a foundry database.

In the next part, the authors describe in detail our proposed methodological framework using the collected data. The framework consists of three main steps; 1) determination of parameter control boundaries, 2) determination of critical process parameters and 3) creation of parameter control models.

### Determination of Parameter Control Boundaries

To ensure consistent casting quality, process parameter values should be kept stable and at the right level. For this, reliable control boundaries (upper and lower control limits) for these parameters are required to help warn the foundry operators. In principle, the foundry has been using experience-based boundaries. However, it was still questionable, whether these boundaries are reliable due to undesirable rejection rate. With the collected process data, the authors came up with a new idea to obtain new reliable

control boundaries. To do this, the data from the production dates where there were no casting defects were extracted from the database with the aid of programming. The authors call this ZD data (zero-defect data), for they delivered only good castings. In principle, process parameter values should be kept within the range of the ZD data for good casting results. However, uncertainty and measurement error (extreme values) should be avoided. Using statistics, the authors calculated the confidence interval (CI) of the part-specific ZD data and considered them as new control boundary. For the control tolerance, the authors created two variants of CI, 1) CI where the ZD data are within two standard deviations  $\sigma$  of the mean of ZD data  $\bar{x}_{ZD}$  or Sigma-2 boundary and 2) CI where the ZD data are within three  $\sigma$  of  $\bar{x}_{ZD}$  or Sigma-3 boundary. Both boundaries are narrower than the range of the original ZD data and can be determined using the following equation:

$$CI = x \pm ZD \pm k \cdot \sigma \quad \text{Eqn. 1}$$

where  $k = 2$  for the Sigma-2 boundary,  $k = 3$  for the Sigma-3 boundary and  $\sigma$  can be calculated using the following equation:

$$\sigma = \sqrt{\frac{\sum_{i=0}^n (x_i - \bar{x}_{ZD})^2}{n - 1}} \quad \text{Eqn. 2}$$

where  $n$  is the number of samples, and  $x_i$  is the measured data.

**Table 1. List of Process Parameters**

Parameters	Symbol	Process	Parameter data source	Frequency of measurement
Return sand temperature	$T_{rs}$	MSP	Sand mixer	Every sand mixture (every 2–3 minutes)
Return sand moisture	$M_{rs}$	MSP	Sand mixer	
Dosed bentonite	$B_d$	MSP	Sand mixer	
Dosed water	$W_d$	MSP	Sand mixer	
Dosed sea coal	$C_d$	MSP	Sand mixer	
Dosed water temperature	$T_{dw}$	MSP	Sand mixer	
Mixing time	$t_{mix}$	MSP	Sand mixer	
Vacuum cooling time	$t_{vac}$	MSP	Sand mixer	
Target sand compactability	$C_t$	MSP	Sand mixer	
Molding sand compactability	$C_{ms}$	MSP	Inline molding sand tester	
Molding sand shear strength	$S_{ms}$	MSP	Inline molding sand tester	
Molding sand temperature	$T_{ms}$	MSP	Pyrometer on sand conveyer	
Molding sand moisture	$M_{ms}$	MSP	Sand laboratory	2 times/shift
Molding sand compressive strength	$CS_{ms}$	MSP	Sand laboratory	
Molding sand bentonite content	$B_{ms}$	MSP	Sand laboratory	
Cast iron chemical compositions: C, Si, Mn, S, P, Cr, Mo, Cu, Mg, Sn, Zn, Ni, Al, Co, Nb, Ti, V, W, Pb, As, Ce, N and Fe	Chem	MIP	Spectrometer and thermal analysis	Every melting charge (every half an hour)
Carbon equivalent	CE	MIP	Thermal analysis	
Liquidus temperature	$T_{liq}$	MIP	Thermal analysis	
Mold compactability	$C_m$	Molding	Molding machine	Every mold (every 15–20 seconds)
Mold thickness	$W_m$	Molding	Molding machine	
Molding line cycle time	$t_{cyc}$	Molding	Molding machine	
Pouring temperature	$T_{pour}$	Pouring	Pyrometer at pouring furnace	
Pouring time	$t_{pour}$	Pouring	Time counter at pouring unit	
Pouring stream width	$W_{pour}$	Pouring	Pouring furnace	
Pouring furnace power	$P_{pf}$	Pouring	Pouring furnace	

*MSP* molding sand preparation and *MIP* molten iron preparation

To give a better view of this, Figure 2 shows that the two boundaries of a sample parameter (mold compactability  $C_m$ ) for a specific casting part can be obtained. The  $C_m$  data from the production batches of the part analyzed with zero-rejection rate (ZD data) are extracted from the database to determine their Sigma-2 and Sigma-3 boundaries. The distribution and the mean (the target value) of the ZD data, together with the resulting boundaries, are shown in Figure 2b.

This procedure can also be applied to other parameters whose data are uniformly distributed to allow monitoring and control of the entire production process. It should be noted that the data used to obtain  $\bar{x}_{ZD}$ , Sigma-2 and Sigma-3 boundaries were cast product-specific, to allow detailed parameter control at product-specific level. Apart from

parameter control purpose, these boundaries could also be used as reference to distinguish between good and bad data, thus helping to identify unstable parameters.

### Determination of Critical Process Parameters

In this part, the authors present the method of identifying critical process parameters (possible reasons of casting defects) without traceability of individual castings. The authors focus on the three main defect groups defined and documented by the foundry which are 1) gas bubbles, sand inclusions and porosities (GSP defects), 2) cold run and 3) broken molds. Ideally, the gas bubbles, sand inclusions and porosities should actually be documented separately in their own defect group. However, such a distinction of

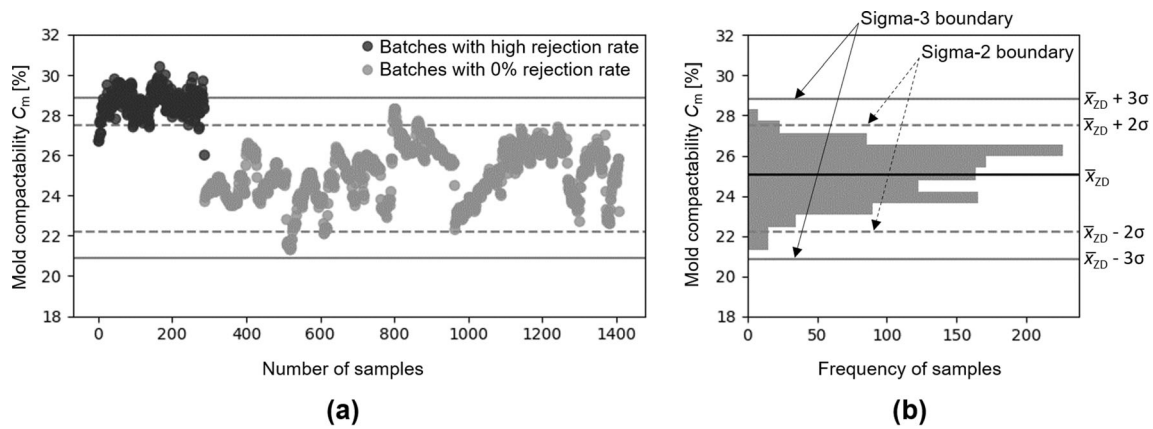


**Figure 2. Mold compactability. (a) Measured data and (b) histogram of the data from the batch with 0% rejection rate and its 95% and 99% confidence intervals (Sigma-2 and Sigma-3 boundaries).**

**Table 2. Chosen Production Batches with High Rejection Rate for Comparative Analysis of Process Data**

Production batch	Cast part	Cast material	Part weight (kg)	Date of production	Casting defect groups	Rejection rate (%)
Batch 1	Water drain grate	GJS-500	5.2	20.04.2018	GSP defects	21
Batch 2	Oven door A	GJL-150	12.5	30.03.2020	GSP defects	45
Batch 3	Oven front wall	GJL-150	22.4	21.09.2021	GSP defects	74
Batch 4	Water drain part	GJS-500	0.9	10.04.2018	Cold run	47
Batch 5	Oven side wall	GJL-150	4.9	11.06.2018	Cold run	50
Batch 6	Oven door plate	GJL-150	3.75	13.10.2020	Cold run	21
Batch 7	Oven door B	GJL-150	21.7	31.03.2020	Broken molds	94
Batch 8	Water drain part B	GJS-500	7.6	22.11.2019	Broken molds	31
Batch 9	Oven door C	GJL-150	10.1	12.02.2020	Broken molds	20

GSP: gas bubbles, sand inclusions and porosities

these defects could not be realized by the shop-floor workers who do not have enough time and metallurgical background for detailed visual inspection of individual parts. Sand inclusions are defects that occur when molding sand particles (torn away by the molten metal stream during pouring process) float to the surface of the casting. Such defects are often inspected on or just under casting surface. Broken molds are defects in shape caused by partial breakage or tearing off of the sand mold during the molding process (mold separation). The defects are caused by the mold that is too brittle and/or excessive compaction with insufficient flowability of the sand.

To describe the analysis method, the authors graphically compared process data between production batches with zero- and high rejection rate in order to identify parameters that show instability. The data were visualized together with the created Sigma-2 and Sigma-3 boundaries generated from the previous step. This should help to visualize the difference in parameter values and point out the causal parameters. For a clear comparison, several production batches with considerably high rejection rate (more than

20%) with a prominent defect group were chosen for the analysis (Table 2). The parameters whose more than 20% of batch data exceed the Sigma-2 boundary (exceedance rate  $ER_{2\sigma} > 20\%$ ) were considered as critical parameters, and they are presented later on in the results and discussion part.

Now for process control, it is important to stabilize the critical parameters by having a good control of their related initial process inputs. In the next part, the authors show a method on how to create some parameter control models using the available production data from the years 2018 to 2020, to help stabilize the quality of molding sand and molten iron. After that, the data from the year 2021 were used for model testing.

### Creation of a Molding Sand Moisture Prediction Model

For green sand casting, moisture content of the molding sand is one of the most important parameters to be well



controlled because of its influence on many molding sand properties such as bonding, flowability, compactability, gas permeability and strength.<sup>8,9</sup> Therefore, dosing the right amount of water during the preparation of a sand mixture is highly important and should be adjusted according to the initial sand condition (the return sand) to achieve final target moisture content. Table 3 shows that the average value of some green sand properties measured and recorded at the sand laboratory during the years 2018–2020.

In the foundry, return sand moisture  $M_{rs}$ , temperature  $T_{rs}$  (initial sand conditions) and the corresponding dosed water  $W_d$  (during the mixing process) were measured inline and recorded for each sand mixture (4 tons/mixture). After analyzing the sand data from the years 2018 to 2020 of a sand mixer (approximately 150,000 mixtures in total), it was found that there were large variations in  $M_{rs}$  and  $T_{rs}$ . The reasons for this could be either changing weather conditions or different settings of sand cooling at the sand recycling plant by different workers. Furthermore, the authors found correlations between  $W_d$  and  $M_{rs}$  as well as  $W_d$  and  $T_{rs}$ , with Pearson correlation coefficient  $r$  of  $-0.76$  and  $0.92$ , respectively (Figure 3a and b). This indicates that  $W_d$  was adjusted according to the initial return sand condition. The higher the  $M_{rs}$ , the lower the  $W_d$ . Conversely, the higher the  $T_{rs}$ , the higher the  $W_d$ . Based on this finding, a regression model with two predictors could be developed.

Due to the noticeable linear characteristic, the authors started by fitting the linear model which gives a coefficient of determination  $R^2$  (the goodness of the model fit, ranging from 0 to 1) of 0.879. Polynomial models of degree of 2, 3 and 4 were also fitted and the resulting  $R^2$  are 0.883, 0.884 and 0.885, respectively, indicating no significant improvement in goodness of fitting over the linear model. Overall, with such a set of comparable  $R^2$ , the linear model was chosen, because it has a much smaller number of regression coefficients which makes it much easier to interpret the influence of each parameter in the real-world application (in this case, the variation of the amount of dosed water during the molding sand preparation process via different regression slopes and intercepts). The linear model shown in Figure 3c can be presented as follows:

$$W_d = \beta_1 \cdot M_{rs} + \beta_2 \cdot T_{rs} + \beta_0 \quad \text{Eqn. 3}$$

where  $\beta_0$ ,  $\beta_1$  and  $\beta_2$  are the regression coefficients.

In summary, there is already a moisture correction system at the foundry to achieve the target molding sand moisture  $M_{ms}$ , and its schematic is presented in Figure 4.

For quality control of  $M_{ms}$ , a cup of molding sand was manually taken from the sand conveyer after mixing process for offline moisture measurement using a digital sand moisture tester at the sand laboratory. However, the measurements were conducted only twice per shift (3–4 measurements per day). In summary, out of 150,000 mixtures, only about 1800 mixtures were with measurement of  $M_{ms}$ . There is no inline measurement to control the  $M_{ms}$  of each mixture.

Nevertheless, the 1800 measured values of  $M_{ms}$  from the sand laboratory allow us to see the variation in the moisture content. Despite the moisture correction system, the variation in  $M_{ms}$  was relatively high (2.80–3.73%). In our view, a solution for more accurate water dosing to reduce the variation in  $M_{ms}$  was needed, and this is where the available collected data and process modeling can support. For this, the authors started to investigate in detail the effect of

**Table 3. Properties of the Green Sand**

Properties	Average measured value
Grain size	0.185 mm
Moisture content $M_{ms}$	3.27%
Compressive strength $CS_{ms}$	21.5 N/cm <sup>2</sup>
Permeability number $P_{ms}$	69
Compactability $C_{ms2}$	38.6%
Bentonite content $B_{ms}$	8.9%

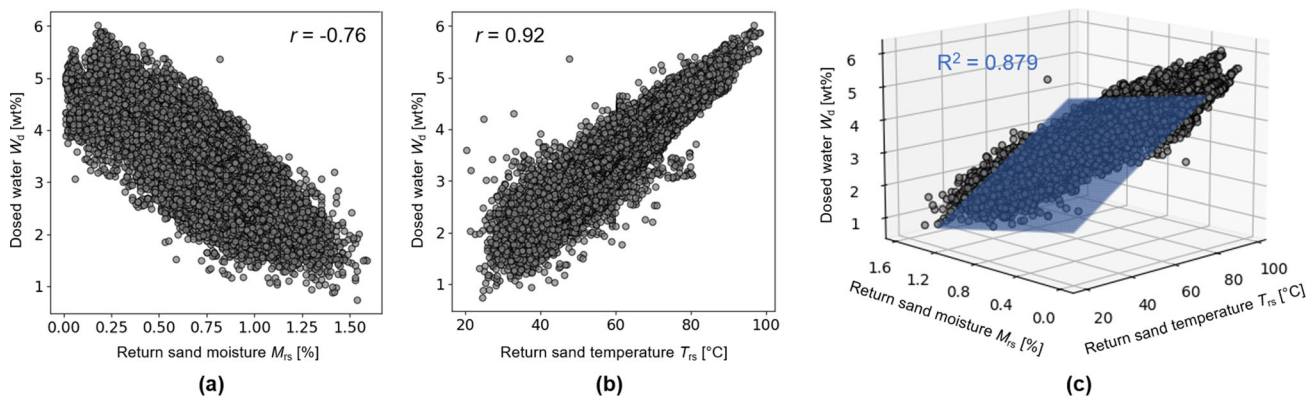


**Figure 3. Correlations between dosed water and return sand parameters. (a) Moisture; (b) temperature and (c) regression model with return sand moisture and temperature as predictors.**

the dosed water  $W_d$  on the molding sand moisture  $M_{ms}$ . The  $M_{ms}$  data from the sand laboratory (of the 1800 mixtures) were classified into five different moisture levels and plotted in five different colors as shown in Figure 5a. According to these levels, five average values of moisture  $\bar{M}_{ms,L1-5}$  were determined. The  $M_{rs}$ ,  $T_{rs}$  and  $W_d$  data of the 1800 sand mixtures were then visualized in 3D scatter plot, colored according to the defined moisture level (Figure 5b).

When fitting regression planes by moisture level, an orderly classification of the data (from low to high moisture) was clearly observed, indicating a direct influence of

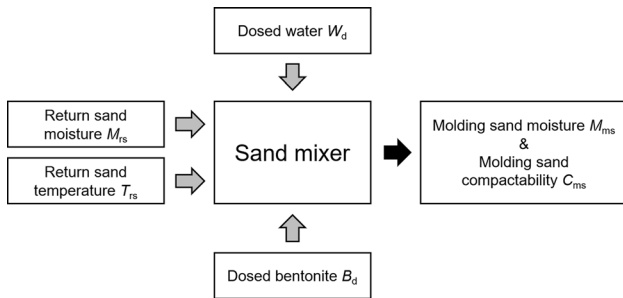
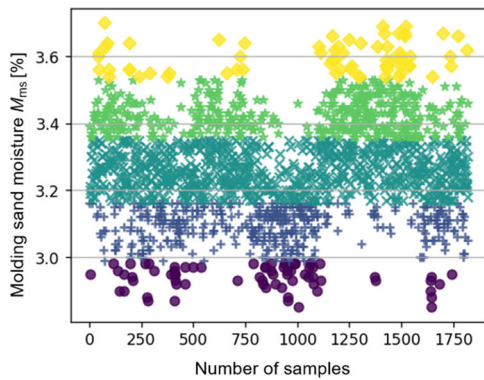
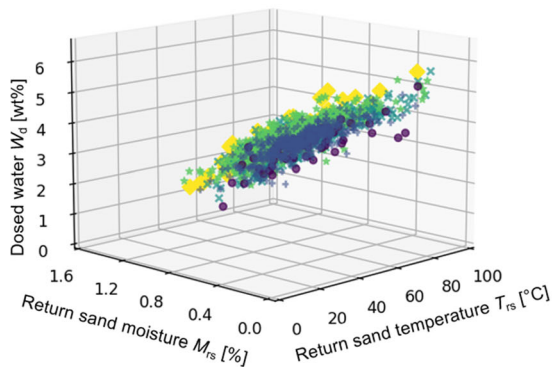


**Figure 4. Schematic of molding sand moisture and compactability correction during the mixing process.**



(a)



(b)

$W_d$  on  $M_{ms}$  (Figure 5c). The equation for these regression planes can be described as follows:

$$W_{d,n} = \beta_{1,n} \cdot M_{rs} + \beta_{2,n} \cdot T_{rs} + \beta_{0,n} \quad \text{Eqn. 4}$$

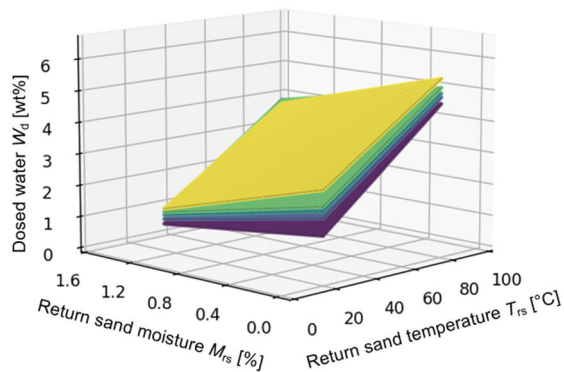
where  $\beta_0$ ,  $\beta_1$  and  $\beta_2$  are the regression coefficients, and  $n$  is the number of moisture levels (1–5).

From the plot, it can be seen that for constant  $M_{rs}$  and  $T_{rs}$ , the higher the  $W_d$ , the higher the  $M_{ms}$ . In addition, at high  $M_{rs}$  and/or  $T_{rs}$ , the change in  $W_d$  becomes more sensitive to the level of  $M_{ms}$  (more difficult to control). On top of that, the plot with regression planes actually allows us to predict the  $M_{ms}$  of a sand mixture. By observing  $M_{rs}$ ,  $T_{rs}$  and  $W_d$  of a sand mixture, it is possible to locate the plane of moisture level in which the data coordinate falls. And from this,  $M_{ms}$  of the coordinate can be estimated by linear interpolation within these five average moisture values ( $\bar{M}_{ms,L1-5}$ ).

To better illustrate this, Figure 6 shows an example of how  $M_{ms}$  of a sand mixture for specific  $M_{rs}$ ,  $T_{rs}$  and  $W_d$  is predicted. In step 1, the five regression models (Eq. 4) are used to determine five different values of the dosed water  $W_{d,L1-5}$ , given return sand conditions ( $M_{rs} = 0.6\%$ ,  $T_{rs} = 50^\circ\text{C}$ ). In step 2, the determined  $W_{d,L1-5}$  from step 1 and the known  $\bar{M}_{ms,L1-5}$  are then paired to create a corresponding linear regression model (Eq. 5), which can be used to

Molding sand moisture  $M_{ms}$  [%]

- Moisture level 1:  $2.80 < M_{ms} \leq 2.98$ ,  $\bar{M}_{ms,L1} = 2.94$
- + Moisture level 2:  $2.98 < M_{ms} \leq 3.17$ ,  $\bar{M}_{ms,L2} = 3.10$
- × Moisture level 3:  $3.17 < M_{ms} \leq 3.35$ ,  $\bar{M}_{ms,L3} = 3.26$
- ★ Moisture level 4:  $3.35 < M_{ms} \leq 3.54$ ,  $\bar{M}_{ms,L4} = 3.43$
- ◆ Moisture level 5:  $3.54 < M_{ms} \leq 3.73$ ,  $\bar{M}_{ms,L5} = 3.61$



(c)

**Figure 5. (a) Measured molding sand moisture; (b) relationship between return sand moisture, temperature and dosed water and (c) fitted regression planes for each moisture level.**

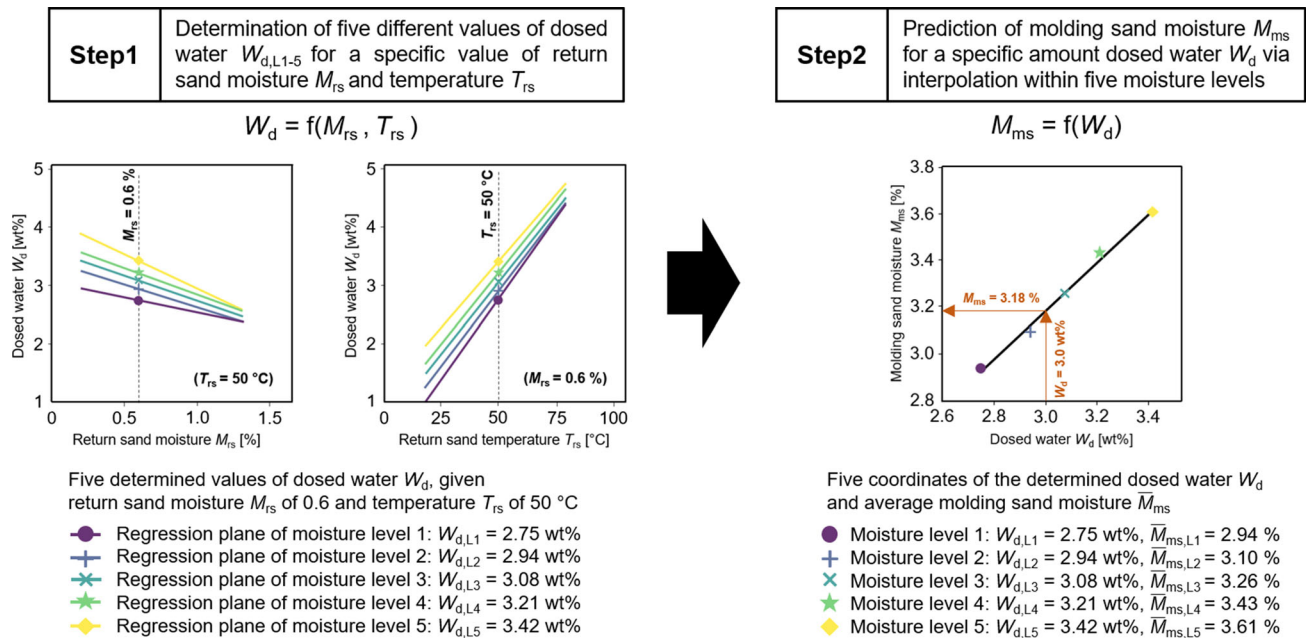


**Figure 6. Molding sand moisture prediction procedure, given initial return sand moisture, temperature and dosed water.**

predict  $M_{ms}$ , given  $W_d$  (the interpolation within five moisture levels).

$$M_{ms} = a \cdot W_d + b \quad \text{Eqn. 5}$$

where  $a$  is the slope and  $b$  is the intercept of the regression, both of which vary by sand mixture due to the changing sand conditions (different  $M_{rs}$  and  $T_{rs}$ ). This linear regression model in step 2 is, therefore, mixture-specific (recreated per mixture). For this example, the model with a slope  $a$  of 1.026 and an intercept  $b$  of 0.103 is created and, with dosed water  $W_d$  of 3.0 wt%, molding sand moisture  $M_{ms}$  of 3.18% is predicted.

More importantly, the five regression models in step 1 also allow us to determine an appropriate amount of dosed water  $W_d$  based on  $M_{rs}$  and  $T_{rs}$  to achieve a specific target  $M_{ms}$ . For this example, if the return sand has a moisture content of 0.6% and a temperature of 50 °C, then to achieve molding sand moisture level 3 ( $M_{rs} = 3.26\%$ ), water of 3.08 wt% ( $W_{d,L3}$ ) should be dosed to the sand mixer. In other words, 123.2 kg of water should be dosed to a 4-ton sand mixture.

Apart from the moisture control, compactability is also one important property of the molding sand and was found to have correlation with the moisture content.<sup>9</sup> In this work, similar correlations were also realized. Figure 7 shows how the molding sand compactability  $C_{ms}$  correlates with the molding sand moisture  $M_{ms}$ , as well as the molding sand bentonite content  $B_{ms}$  (offline measurement with equipment at the sand laboratory, ranging from 8.0 to 9.9%). The higher the  $M_{ms}$ , the higher the  $C_{ms}$ . On the contrary, the higher the  $B_{ms}$ , the lower the  $C_{ms}$ . Besides, at low  $M_{ms}$ , the

$B_{ms}$  has stronger influence on  $C_m$ , which aligns with the past work.<sup>10</sup> The relationship (Figure 7b) allows quantitative control of the  $C_{ms}$  based on dosed water  $W_d$  and dosed bentonite  $B_d$ . At the foundry, the bentonite additions was manually adjusted once per sand cycle based on the measured compressive strength of the mixed sand  $CS_{ms}$  (measured offline by the sand mixer operators). Based on the  $CS_{ms}$ , the operators decide from experience how much bentonite is added to the system. The higher the  $CS_{ms}$ , the lower the bentonite added to the system and vice versa.

### Creation of a Liquidus Temperature Prediction Model

Producing good castings requires not only quality control of the molding material but also of the casting material. Many past works reported that casting defects, such as shrinkage, are associated with liquidus temperature and carbon equivalent of the melt.<sup>11,13,14</sup> To avoid such defects and premature solidification of the melt (risk of cold run defect), the authors proposed models to control the liquidus temperature of the melt  $T_{liq}$  for each type of iron (GJL, GJV and GJS) using the data from spectral and thermal analysis, performed at the foundry. For this, the carbon equivalent CE from spectrometer, calculated on the basis of carbon content C, silicon content Si and phosphorus content P ( $CE = C + Si/4 + P/2$ ), was used as the independent variable and  $T_{liq}$  as the dependent variable of the model.

Based on the scatter of the data (Figure 8), there exists a clear negative correlation between CE and  $T_{liq}$  at CE <



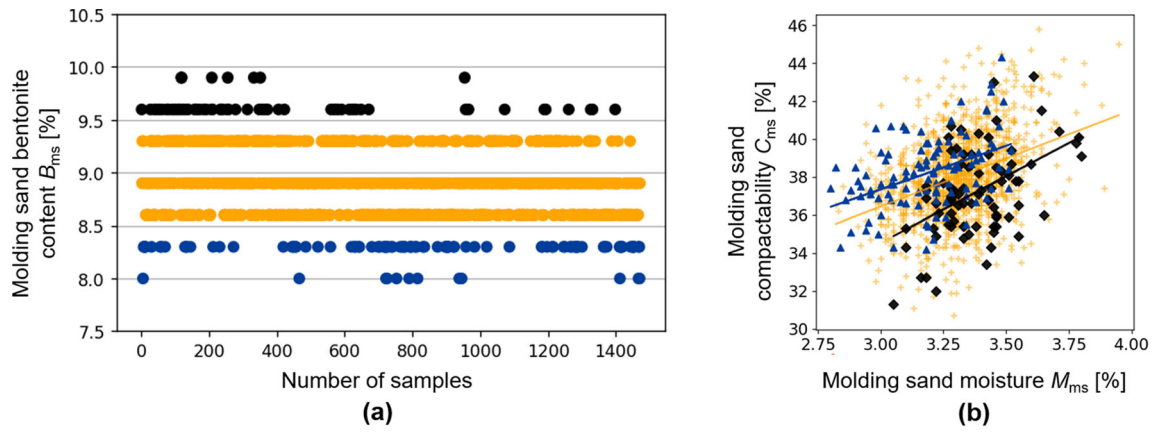


**Figure 7. Correlation between the resulting molding sand moisture, bentonite content and compactability.**

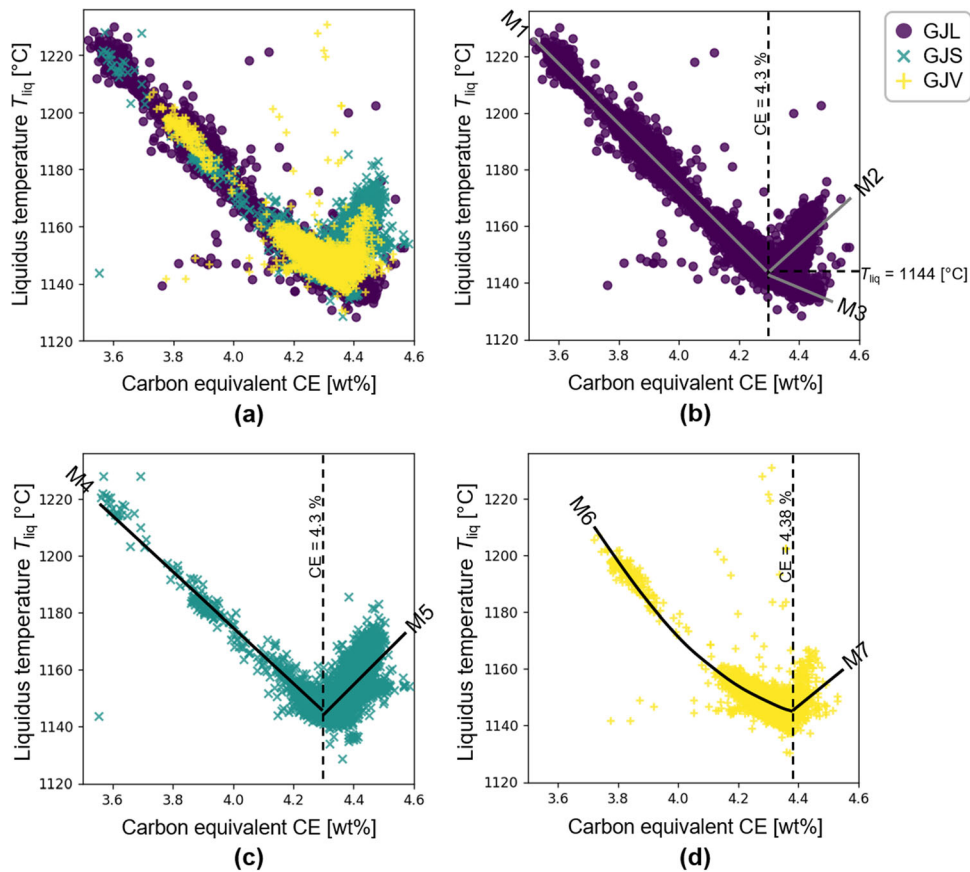


**Figure 8. Correlations and regression models for predicting and controlling liquidus temperature of the three different irons (GJL, GJS and GJV) based on carbon equivalent.**

4.3% which is consistent with the past work.<sup>15</sup> For accurate prediction, the authors decided to fit seven different regression models, which covers prediction for hypoeutectic, eutectic and hypereutectic compositions for all irons. Similar to the past work and the Fe–C phase diagram, the GJL and GJS irons show an eutectic point at CE  $\approx$  4.3%.<sup>11,12</sup> Whereas, the GJV iron shows a slightly different eutectic point at CE  $\approx$  4.38%. Moreover, the hypoeutectic

compositions for GJV iron show a nonlinear correlation between CE, and the authors decided to fit a polynomial model of degree of 2.

The models for GJL (M1, M2 and M3), GJS (M4 and M5) and GJV (M6 and M7), created using data from the years 2018 to 2020, were then tested for their prediction performance using another set of data from the year 2021, and

the results are presented later on in the results and discussion section. The equations obtained for all the models are as follows:

Model M1 (for GJL with CE  $\leq 4.3$  %):

$$T_{liq} = -105.98CE + 1599$$

Eqn. 6

Model M2 (for GJL with CE  $> 4.3$  % and T<sub>liq</sub>  $\geq 1144$  °C):

$$T_{liq} = 93.355CE + 742.74$$

Eqn. 7

Model M3 (for GJL with CE  $> 4.3$  % and T<sub>liq</sub>  $< 1144$  °C):

$$T_{liq} = -44.073CE + 1332.4$$

Eqn. 8

Model M4 (for GJS with CE  $\leq 4.3$  %):

$$T_{liq} = -97.164CE + 1563.3$$

Eqn. 9

Model M5 (for GJS with CE  $> 4.3$  %):

$$T_{liq} = 106.32CE + 687.31$$

Eqn. 10

Model M6 (for GJV with CE  $\leq 4.38$  %):

$$T_{liq} = 105.76CE^2 - 955.48CE + 3300.9$$

Eqn. 11

Model M7 (for GJV with CE  $> 4.38$  %):

$$T_{liq} = 86.974CE + 764.85$$

Eqn. 12

## Model Validation

For model validation, the models for predicting molding sand moisture  $M_{ms}$  and liquidus temperature  $T_{liq}$ , created using the data from the years 2018 to 2020, were tested with another set of production data from the year 2021. To evaluate accuracy of the models, the root-mean-square error (RMSE), which is the standard deviation of the prediction errors, was used. The RMSE shows how far the predicted values  $\hat{y}_i$  are from the measured values  $y_i$ . The closer the RMSE is to zero, the better the prediction performance of the model. The RMSE can be calculated as follows:

$$RMSE = \sqrt{\frac{\sum_{i=0}^N (y_i - \hat{y}_i)^2}{N}}$$

Eqn. 13

where  $N$  is the number of test samples.

## Results and Discussion

### Critical Process Parameters Based on the GSP Defect

In order to investigate the possible cause of GSP defects, the process data of Batches 1–3 were visualized in comparison with zero-defect batches. As a result, the batch data

of the parameters with an exceedance rate  $ER_{2\sigma}$  of more than 20% (the critical parameters) are shown in Figure 9. The result indicates that there could be several reasons of the GSP defects. Too high bentonite content was observed (Batch 1), which is consistent with the fact that too much binding material can lead to insufficient permeability of the molding sand (poor ventilation of gases formed during pouring) and thus gas porosities and bubble-like surface defects (GSP defect group).<sup>16,17</sup> Furthermore, too high molding sand temperature was observed (Batch 2), which is consistent with DISA's molding sand instruction manual that this can lead to non-uniform sand permeability and strength, as well as decreased mixability.<sup>18</sup> Additionally, too high mold compactability was observed (Batch 3), which is consistent with the fact that it leads to high deformability of the molds, dimensional variation and thus an increased chance of shrinkage defects.<sup>19,20</sup> For the melt, irons with relatively high phosphorus content were observed (Batch 1), which is consistent with the fact that it can negatively impact the properties of ductile iron and cause shrinkage porosities.<sup>21,22</sup> Moreover, irons with too low carbon equivalent CE were observed (Batch 2), which is consistent with an existing report that low CE iron promotes low graphite expansion during solidification and thus insufficient material volume to push out existing shrinkage porosities in castings.<sup>23</sup>

### Critical Process Parameters Based on the Cold Run Defect

Next, the batches with high rate of cold run defect (Batches 4–6) were analyzed. Cold run defect can be seen on the surface of the casting and is caused by premature solidification of the melt during casting.<sup>24</sup> Based on the analysis result, too low pouring temperature (Batches 5 and 6), too low carbon equivalent CE and/or too high liquidus temperature (Batch 4) are associated with the cold run defect (Figure 10). This is consistent with the fact that all of these factors usually promote premature solidification and thus the risk of cold run.<sup>19,25</sup>

### Critical Process Parameters Based on the Broken Molds Defect

The batches with high rejection rate due to broken molds (Batches 7–9) were analyzed. Broken molds defect is visible on the cast part surface with large cuds and occur when the separation resistance of the molding sand is greater than its strength (too high compaction and/or too low sand strength).<sup>26</sup> From the analysis result, it was observed that for the same value of the return sand moisture  $M_{rs}$ , the dosed water in the sand mixer of the defective batches (Batches 7–9) were noticeably higher than that of the batches with no defect (Figure 11a–c). In other words, an excessive amount of dosed water appears to be associated

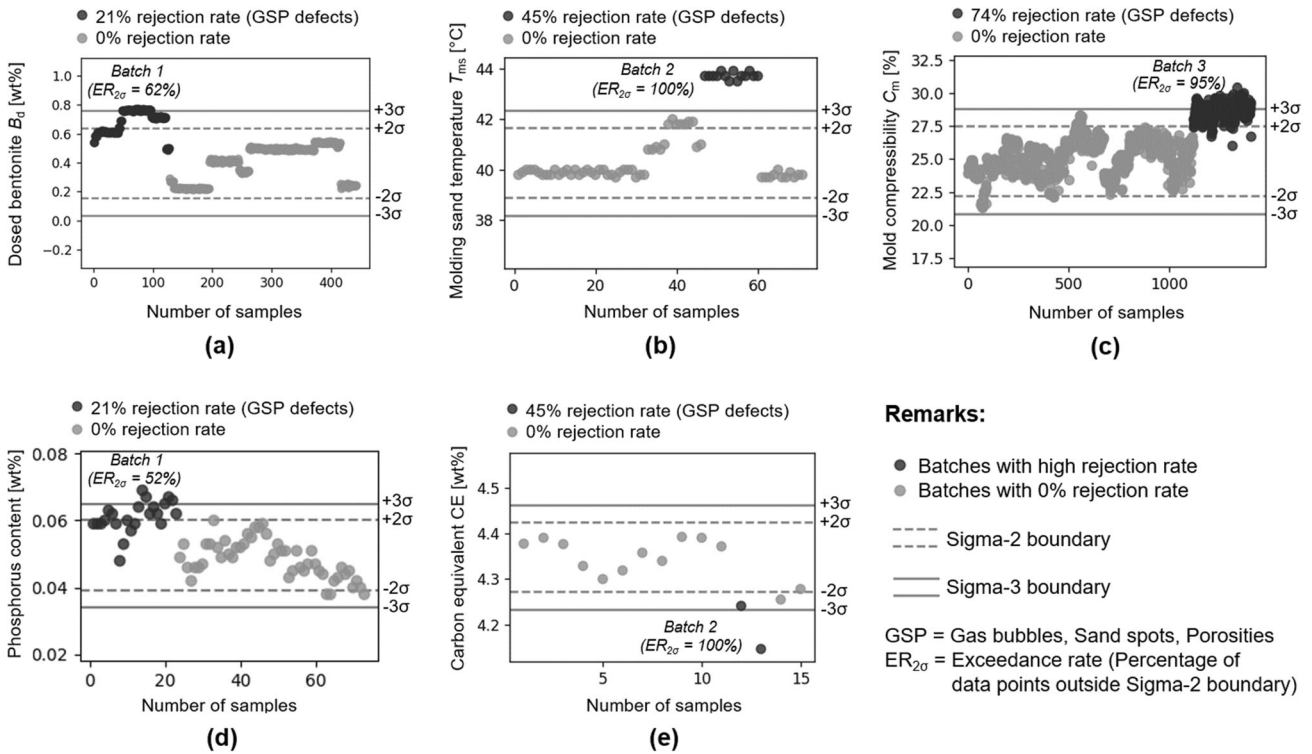


**Figure 9. Scatter plots of unstable inline parameters based on GSP defects in comparison with zero-defect batches.**

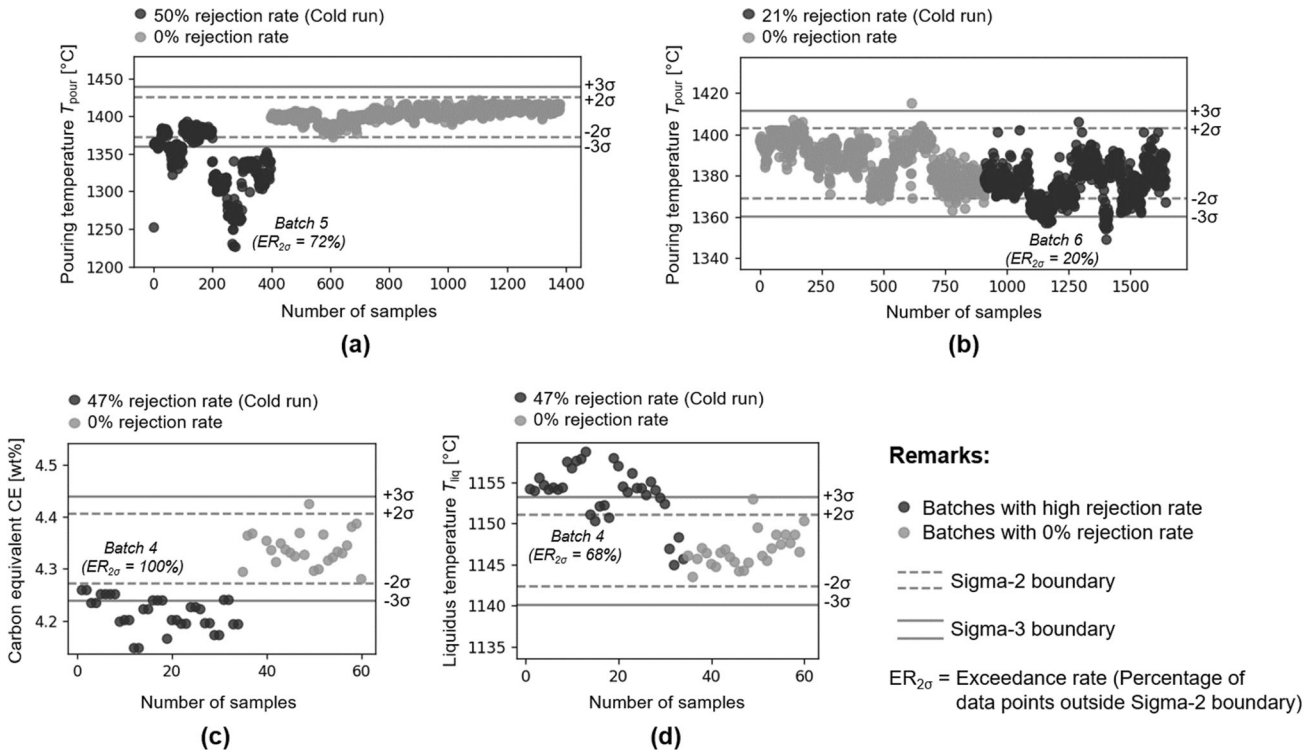


**Figure 10. Scatter plots of unstable inline parameters based on cold run defect in comparison with zero-defect batches.**

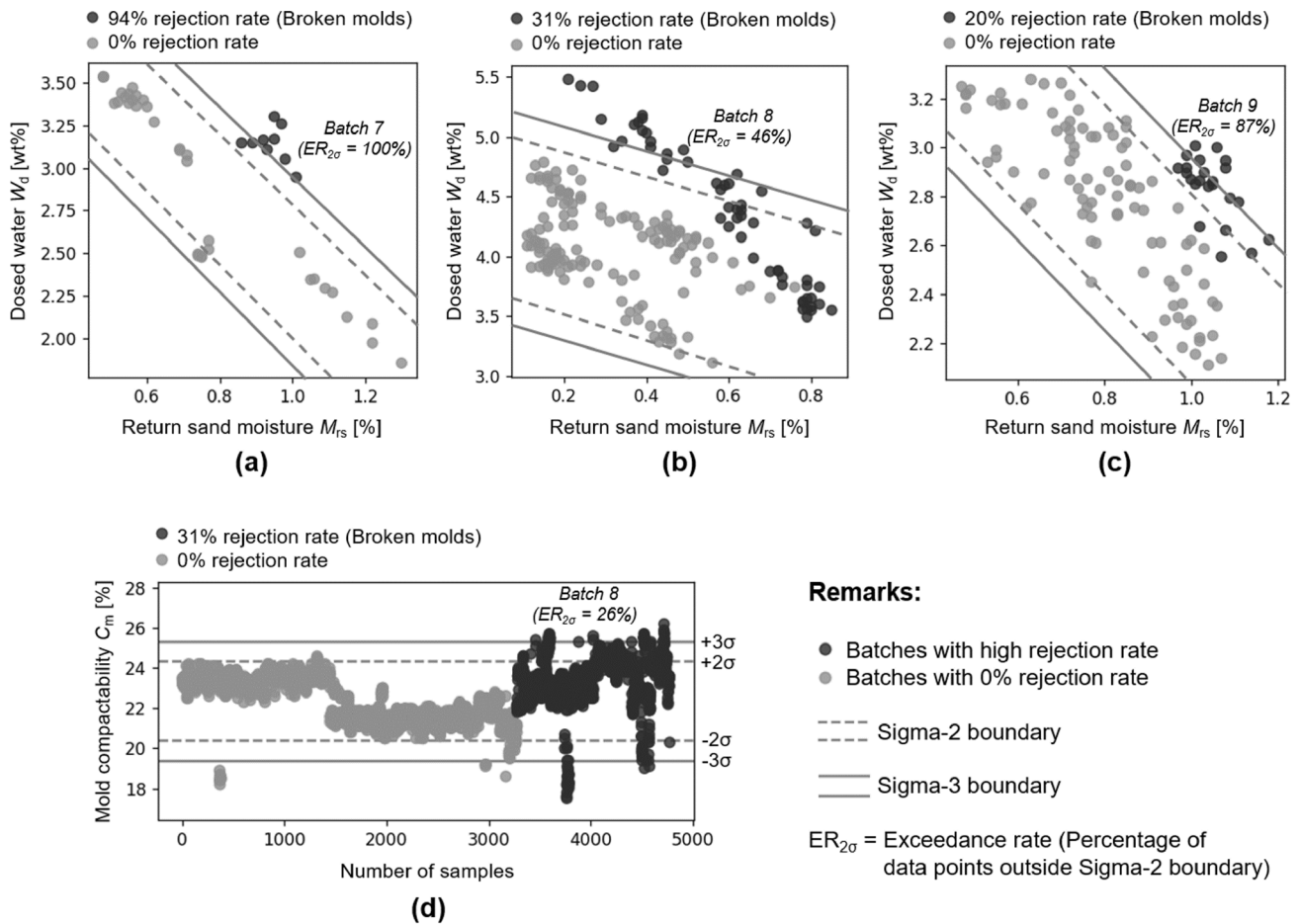


**Figure 11. Scatter plots of unstable inline parameters based on broken molds defect in comparison with zero-defect batches.**

with the broken molds defect. Additionally, the data of Batch 8 show a large variation in the mold compactability (Figure 11d). These results are consistent with the fact that the mold can break during the molding or pouring process, if the moisture and/or compactability of the molds is too low (dry and friable) or too high (low strength and high deformability).<sup>19</sup>

The comparison of inline process data between batches with zero- and extremely high rejection rate allows us to see a distinctive degree of data variation, especially when visualizing with the created confidence interval (CI) of the ZD data (Sigma-2 and Sigma-3 boundaries). As a result, the authors were able to identify the process parameters that are sensitive to casting defects, even though the inline data of individual outgoing parts could not be traced. Regardless of the defect groups, it is in any case very important that the foundry can maintain the values of these parameters within the created boundaries to ensure good castings. The analysis also shows that the Sigma-2 boundary can be a good reference to classify the data between good and defective batches. Therefore, it is recommended to keep inline process data within the Sigma-2 boundary.

### Control Issue in Sand Preparation System

Due to the high variability of the sand data, especially the resulting sand moisture and compactability, further investigation on molding sand preparation system was conducted. This was done by visualizing the sand data recorded during the production of a specific oven door casting over different batches (A–G) (Figure 12). It was found that the target compactability  $C_t$  (Figure 12c) was being changed, which should not be the case, as this affects the moisture correction. It was realized that the mixer operators also do offline measurements of the resulting molding sand compactability once per sand cycle (approximately every 20 mixtures) and then change the target compactability  $C_t$  based on what was measured to strengthen or weaken the existing moisture and compactability correction of the system. This appears to be a double moisture correction (one by the system and one by the operators), which could be the cause of the high variability in the resulting molding sand compactability  $C_{ms}$  and  $C_m$  (Figure 12f and g). In addition, Figure 12e (Batch A) shows insufficient bentonite addition, resulting in higher level shift of  $C_{ms}$  and  $C_m$ . This is consistent with the correlation found (Figure 7b) and past work.<sup>10</sup> A solution to



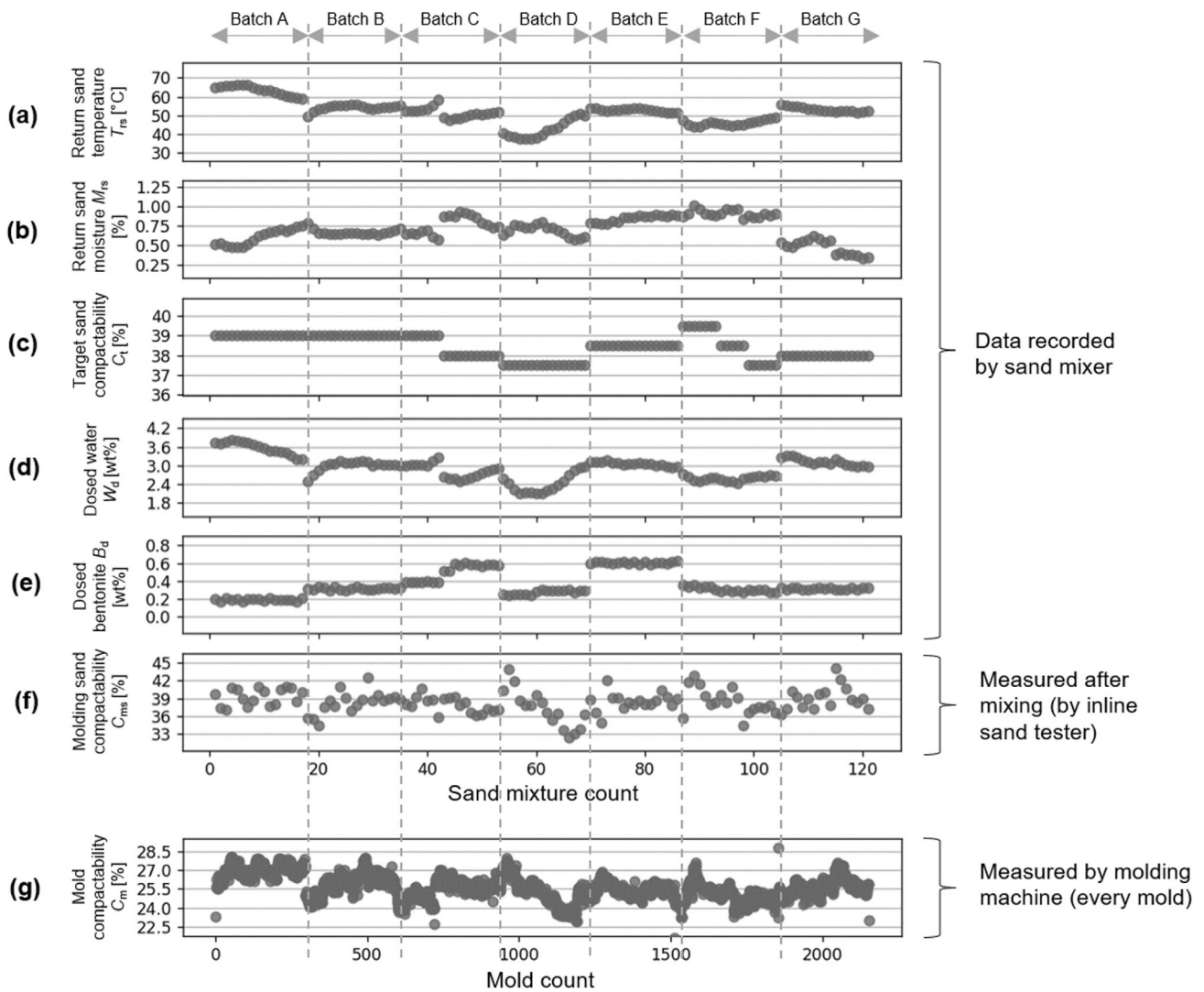


**Figure 12.** Scatter plots of molding sand data during production of a specific oven door casting from different batches.

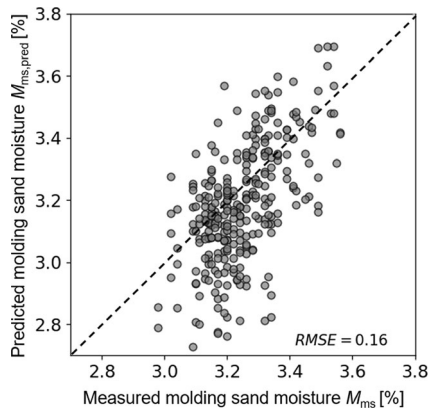


**Figure 13.** Correlation between the measured and predicted molding sand moisture.

this could be the installation of inline measurement of the return sand compressive strength (compared to the mixed sand compressive strength and bentonite content) in order

to estimate a correct bentonite addition during the mixing process.

### Model Performance

Based on the test result, the model for predicting molding sand moisture  $M_{ms}$  has an RMSE of 0.16%, which is not a small number, considering the range of measured  $M_{ms}$  between 2.80 and 3.73%, but still less than a standard deviation of the moisture data (0.17%). The first reason for the error could be the fact that the moisture probe at the sand mixer does not always measure the correct value due to sand accumulating on the probe over time. Another reason could be due to the uncertainty in the offline moisture measurement at the sand laboratory due to non-uniform sand mixture, moisture loss during transport of the sample sand and seasonal changes. A comparison of the measured and predicted molding sand moisture is shown in Figure 13. The diagonal line indicates the minimum

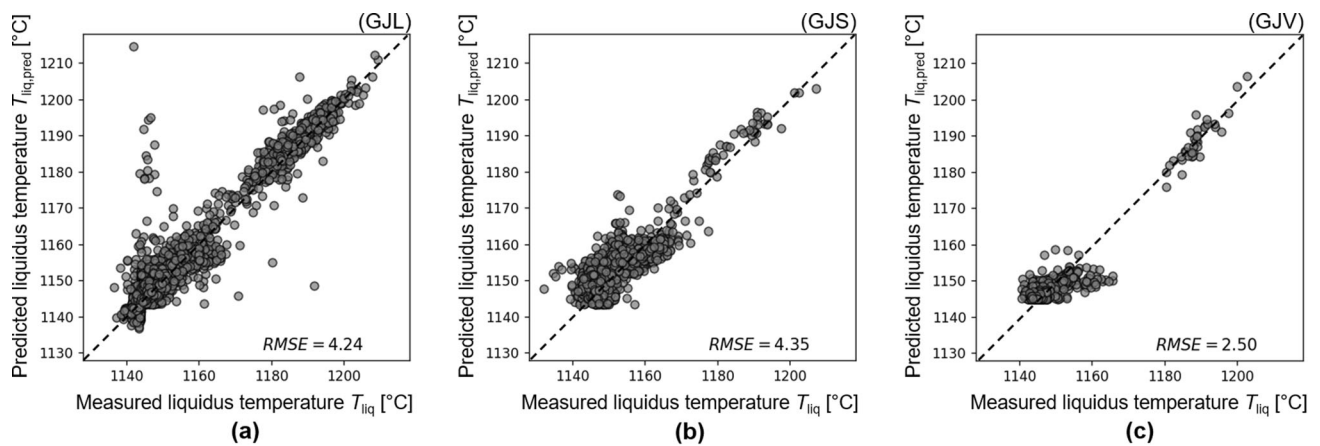


**Figure 14. Correlations between the measured and predicted liquidus temperature of the melt.**

difference between measurement and prediction. The smaller the data spread around the diagonal line, the smaller the RMSE and therefore the better the prediction performance.

Although the offline measurement of molding sand moisture at the sand laboratory is carried out only 3–4 times a day, over a period of 3 years, it has provided sufficient amount of data (from 1800 mixtures) to create useful models for parameter control. The first benefit for the foundry is that the model can be used to predict and control the  $M_{ms}$  of all prepared sand mixtures by observing the initial sand conditions (return sand moisture and temperature) and the dosed water, instead of spending additional costs on a new inline sand moisture sensor.<sup>27</sup> Secondly, more precise control of the dosed water based on the initial sand conditions (Eq. 4) helps to achieve more stable molding sand moisture. In order to reduce the variability in the resulting molding sand moisture and compactability, the foundry should avoid the situation shown in Figure 12c (changing target molding compactability  $C_t$ ).

For the prediction of liquidus temperature of the melt  $T_{liq}$  based on carbon equivalent CE, the models for GJL, GJS and GJV irons show good prediction performance with RMSE of 4.24, 4.35 and 2.50 °C, respectively. The RMSE values are less than the standard deviation of the measured  $T_{liq}$  (8.8 °C), which is accurate enough for use in predictive process control. According to the correlation between the measured and predicted  $T_{liq}$  shown in Figure 14, the prediction errors are relatively higher at low  $T_{liq}$  (below 1160 °C) for all irons. This is due to the unclear correlation between CE and  $T_{liq}$  in the hypereutectic composition zone (see Figure 8).

The models with CE as a predictor allow quantitative control of  $T_{liq}$  based on the chemical elements C, Si and P. Last but not least, it is important to note that irons with high  $T_{liq}$  are prone to premature solidification of the melt (risk of cold run defect), if the pouring temperature  $T_{pour}$  is

kept constant. For this reason, the  $T_{liq}$  prediction model is, therefore, very helpful for foundry operator in setting the right  $T_{pour}$  for each melt according to  $T_{liq}$ .

Overall, this work focuses on stabilizing the key inline parameters within the determined boundaries (confidence interval of zero-defect data) and creating their target functions, rather than attempting to establish a direct relationship between initial process inputs and cast part quality (which requires experimental design or complete process traceability). In industrial practice, if the quality of the molding sand, the melt and the pouring data are met as they were from the zero-defect batches, then good castings can be expected. This method of data analysis and modeling is not limited to only green sand casting, but should also be applicable to other casting processes and even to those from other manufacturing industries.

## Conclusion

This paper presents a methodological framework on how to utilize casting production data from a sand foundry in order to identify critical process parameters create a data-driven process control. Based on the work outcomes, the following conclusions were drawn:

- Despite the limitation of complete process traceability, critical parameters could be identified with the aid of the comparative analysis (data visualization and comparison between production batches with zero- and high rejection rate).
- Unstable molding sand temperature  $T_{ms}$  and compactability  $C_{ms}$  were found to be the possible reasons of GSP (gas bubbles, sand inclusions and porosities) and broken molds defects.
- Unstable phosphorus content P, carbon equivalent CE, liquidus temperature  $T_{liq}$  and pouring temperature  $T_{pour}$  were found to be the possible reasons of GSP and cold run defects.

- Parameter control boundaries (upper and lower limits) for each process parameter were determined by calculating the confidence interval CI of the data from the production dates with zero rejection (ZD data).
- The Sigma-2 boundary (CI where the ZD data are within two standard deviations of the mean of the ZD data) was found to be a good separator between good and defective production batches.
- With the molding sand data provided, the authors were able to create a molding sand moisture prediction model with a prediction error RMSE of 0.16%. The cause of the error could be an inaccurate measurement of the return sand moisture by a moisture sensor at the sand mixer due to sand being stacked over time.
- With the iron data provided, the authors were able to create a liquidus temperature prediction model for each iron (GJL, GJS and GJV) with RMSE of 2.50–4.35 °C, which is acceptable considering the range of  $T_{liq}$  between 1137 and 1230 °C with standard deviation of 8.80 °C.
- The foundry could save the cost of procuring new sensors by using the models as soft sensors instead for online prediction and parameter control.

As a suggestion for future work, the implementation of traceability of individual castings at the foundry will definitely be helpful for accurate root cause analysis and better process model performance. Several part marking methods for tracking aluminum alloy parts with cost evaluation were introduced,<sup>28</sup> and it would be interesting to apply the concept to iron castings as well. To ensure the overall monetary benefit of scrap reduction, traceability should be implemented at a fair cost.

### Acknowledgement

The corresponding author would like to thank the foundry Ortrander Eisenhütte GmbH for providing the data and information support.

### Funding

Open Access funding enabled and organized by Projekt DEAL. No funding was received for conducting this study.

**Conflict of interest** The authors have no competing interests to declare that are relevant to the content of this article.

**Open Access** This article is licensed under a Creative Commons Attribution 4.0 International License, which permits use, sharing, adaptation, distribution and reproduction in any medium or format, as long as you give appropriate credit to the original author(s) and the source, provide a link to the Creative Commons licence, and indicate if changes were made. The images or other third party material in this article are included in the article's Creative Commons licence, unless indicated otherwise in a credit line to the material. If material is not

included in the article's Creative Commons licence and your intended use is not permitted by statutory regulation or exceeds the permitted use, you will need to obtain permission directly from the copyright holder. To view a copy of this licence, visit <http://creativecommons.org/licenses/by/4.0/>.

### REFERENCES

1. A. Joshi, L.M. Jugulkar, Investigation and analysis of metal casting defects and defect reduction by using quality control tools, in *Proceedings of IRF International Conference, Goa*, pp. 86–91 (2014)
2. R. Sika, P. Popielarski, Methodology supporting production control in a foundry applying modern DISAMATIC molding line. MATEC Web Conf. **137**, (2017). <https://doi.org/10.1051/mateconf/201713705007>
3. G.G. Patil, K.H. Inamdar, Prediction of casting defects through artificial neural network. *Int. J. Sci. Eng. Technol.* **2**(5), 298–314 (2014)
4. M. Perzyk, A. Kochański, Detection of causes of casting defects assisted by artificial neural networks. *J. Eng. Manuf.* **217**(9), 1279–1284 (2003). <https://doi.org/10.1243/095440503322420205>
5. N.K. Vedel-Smith, T.A. Lenau, Casting traceability with direct part marking using reconfigurable pin-type tooling based on paraffin-graphite actuators. *J. Manuf. Syst.* **31**(2), 113–120 (2012). <https://doi.org/10.1016/j.jmsy.2011.12.001>
6. Digitale Impressionen der GIFA 2019 - Ist das alles schon einsatzbereit? Die vernetzte Gießerei hautnah (2019). <https://www.noricangroup.com/de-de/new-at-norican/norican-news/digital-impressions-from-gifa>. Accessed 27 Jul 2019. (In German)
7. Cision, Tupy becomes first foundry to adopt SinterCast Cast Tracker technology, Press Release (2019), <https://news.cision.com/sintercast/r/tupy-becomes-first-foundry-to-adopt-sintercast-cast-tracker-technology,c2847497>. Accessed 24 Jun 2019
8. F. Edoziuno, O.G. Utu, C.C. Nwaeju, Variation of moisture content with the properties of synthetic moulding sand produced from river Niger sand (Onitsha deposit) and Ukpok Clay. *Int. J. Res. Adv. Technol.* **3**(2), 102–106 (2017)
9. J.O. Aweda, Y.A. Jimoh, Assessment of properties of natural moulding sands in Ilorin and Ilesha, Nigeria. *J. Res. Inf. Civ. Eng.* **6**(2), 68–77 (2009)
10. J. Sadarang, R.K. Nayak, I. Panigrahi, Effect of binder and moisture content on compactibility and shear strength of river bed green sand mould. *Mater. Today Proc.* **46**(11), 5286–5290 (2021). <https://doi.org/10.1016/j.matpr.2020.08.640>
11. V. E. A. Anjos, Use of thermal analysis to control the solidification morphology of nodular cast irons and reduce feeding needs, PhD dissertation, Universität Duisburg-Essen (2015).

12. D. Horstmann, Das Zustandsschaubild Eisen-Kohlenstoff und die Grundlagen der Wärmebehandlung der Stähle, Verlag Stahleisen (1985). **(In German)**
13. A. Regordosa, N. Llorca-Isern, J. Sertucha, J. Lacaze, Evolution of shrinkage with carbon equivalent and inoculation in ductile cast irons. *Mater. Sci. Forum.* **925**, 28–35 (2018). <https://doi.org/10.4028/www.scientific.net/MSF.925.28>
14. Ductile Iron Society, Ductile iron quality assurance guide, <https://mmsallaboutmetallurgy.com/2018/08/25/ductile-iron-quality-assurance-guide/>
15. D.M. Stefanescu, Analysis of the rationale and accuracy of the use of carbon equivalent and thermal analysis in the quality control of cast Iron. *Inter Metalcast* **16**, 1057–1078 (2022). <https://doi.org/10.1007/s40962-021-00685-6>
16. F.O. Aramide, S. Aribo, D.O. Folorunso, Optimizing the moulding properties of recycled Ilaro silica sand. *Leonardo J. Sci.* **19**(1), 93–102 (2011)
17. P.O. Atanda, O.E. Olorunniwo, K. Alonge, O.O. Oluwole, Effect of bentonite and cassava starch on the moulding properties of silica sand. *Int. J. Mater. Chem.* **2**(4), 132–136 (2012)
18. DISA A/S, Disa foundry technology - Molding sand, DISA (1988), p. 17
19. J. Sertucha, J. Lacaze, Casting defects in sand-mold cast irons—an illustrated review with emphasis on spheroidal graphite cast irons. *Metals* **12**(3), 504 (2022). <https://doi.org/10.3390/met12030504>
20. AFS Institute (Schaumburg, Illinois), Defect detective: common green sand flaws. *Modern casting*, 24 (2018)
21. P.M. Ingole, A.U. Awate, S.V. Saharkar, Effect of basic chemical element in Sgi (Ductile Iron). *Int. J. Eng. Res. Technol.* **1**(7), (2012)
22. S. Singh, R. Khanna, N. Sharma, Study and control of factors influencing casting shrinkage using DOE and numerical simulation. *IOP Conf. Ser.: Mater. Sci. Eng.* **624**, (2019). <https://doi.org/10.1088/1757-899X/624/1/012021>
23. W.O. Umezurike, Onche, Experimental analysis of porosity in gray iron castings. *Glob. J. Res. Eng.* **10**(7), 65–70 (2010)
24. V. Ingle, M. Sorte, Defects, root causes in casting process and their remedies: Review. *Int. J. Eng. Res. Appl.* **7**(3), 47–54 (2017). <https://doi.org/10.9790/9622-0703034754>
25. B.R. Jadhav, S.J. Jadhav, Investigation and analysis of cold shut casting defect and defect reduction by using 7 quality control tools. *Int. J. Adv. Eng. Res. Stud.* **2**(3), 28–30 (2013)
26. Ballenabrisse (2022), <https://www.giessereilexikon.com/giesserei-lexikon/Encyclopedia/show/ballenabrisse-43/?cHash=a955b346dbf97667b61c1d60b4fb3d8a>. Accessed 10 Sep 2022 **(In German)**
27. MoistTech Online-Feuchtmessungssensoren (2022), <https://www.promati.com/files/uploads/2022/05/MoistTech-Feuchtemessung-und-regelung.pdf>. Accessed 21 Oct 2022 **(In German)**
28. F. Deng, R. Li, S. Klan, W. Volk, Comparative evaluation of marking methods on cast parts of Al–Si alloy with image processing. *Inter Metalcast* **16**, 1122–1139 (2022). <https://doi.org/10.1007/s40962-021-00661-0>

**Publisher's Note** Springer Nature remains neutral with regard to jurisdictional claims in published maps and institutional affiliations.